Decentralized Collective Transport along Manifolds Compatible with Holonomic Constraints by Robots with Minimal Global Information

Hamed Farivarnejad and Spring Berman

***Abstract*— We present a decentralized adaptive control strategy for collective payload transport by differential-drive robots with manipulator arms. The controllers only require robots' measurements of their own heading and velocity and their manipulator angle and angular velocity, and the only information provided to the robots is the target speed and direction of transport. The control strategy does not rely on inter-robot communication, prior information about the load dynamics and geometry, or knowledge of the number of robots and their distribution around the payload. We first design the desired manifolds of motion for the entire system such that they are compatible with the holonomic constraints between the robots and the payload. Then, we design adaptive controllers for a team of differential-drive robots that initially grasp a payload in an arbitrary configuration. We also analytically establish the stability and convergence of the system trajectories to the desired payload motion. We demonstrate the effectiveness of the proposed controllers through 3D physics simulations with realistic dynamics.**

I. Introduction

Autonomous multi-robot systems have many potential applications in cooperative manipulation tasks that are conducted in GPS-denied, unstructured, uncertain environments. This type of task can arise in scenarios such as search-and-rescue operations, disaster response, and assembly, transport, and construction in remote or hazardous environments. Such applications will require robot control strategies that rely on minimal information and are robust to uncertainties in the payload dynamics. Toward this end, we present, analyze, and simulate a novel decentralized control scheme based on an adaptive control approach. We develop controllers that are comprised of two components, a stabilizing term and a regression-based term which is updated by an adaptation law.

A variety of control methods have been proposed for collective transport tasks in which there is no inter-robot communication. Some of these are leader-follower schemes, such as the control approaches presented in [2], [3], [4]. Other works consider the scenario in which all robots in the transport team are assumed to have the same type of information and follow identical controllers, which is the case that we address in this paper. In [5], a decentralized approach to cooperative transport is proposed in which the load is significantly larger than the robots, which push the load to the goal when their line of sight to the goal is occluded by the load. The works in [6] and [7] consider

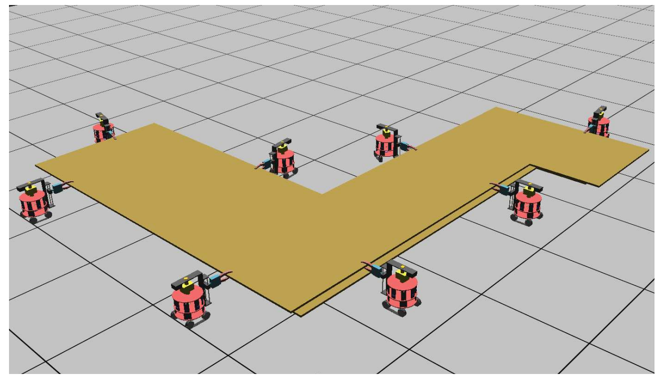

Fig. 1. Simulated Pheeno robots [1] performing a collective transport task.

transport of a flexible load, in which the reaction force between the robot and the load is modeled as the gradient of a nonlinear potential that describes the load deformation. In [8], the load weight is distributed among robots with heterogeneous load-carrying capabilities, and the load is driven along a desired trajectory. Robot control policies that replicate collective transport behaviors observed in ants are proposed in [9], [10]. In [11], all the robots know the target direction to the goal, and a simple control law, which uses just the velocity of the attachment point, is employed. In a similar scenario, decentralized PID controllers are developed in [1] for collective transport by small mobile robots. In the case of aerial collective transport, [12] develops an augmented adaptive sliding mode controller for manipulators mounted on aerial vehicles.

The present work is an extension to our previous papers [13], [14], in which we considered collective transport scenarios that are similar to those in [1] and [11]. In those works, we designed decentralized controllers for teams of point-mass robots that are rigidly attached to the payload. The controllers only required robots' measurements of their own speed and heading, without any information about the number of robots, the payload dynamics, and the robots' distribution around the payload. Here, we consider a more realistic scenario in which the collective transport task is performed by differential-drive robots with 1-DOF manipulator arms, like the robots in Fig. 1.

To derive decentralized controllers that can be implemented on such robots, we make significant modifications to our previous controller design procedure in [13], [14]. Since the robots and their manipulator arms may in general have different initial configurations (see Fig. 1), we must explicitly account for the holonomic constraints between the

This research was supported by ONR Young Investigator Award N00014-16-1-2605.

Hamed Farivarnejad and Spring Berman are with the School for Engineering of Matter, Transport and Energy, Arizona State University (ASU), Tempe, AZ 85287, USA {Hamed.Farivarnejad, Spring.Berman}@asu.edu

robots and the payload in the design of the desired manifolds of motion. To this end, we first design the manifolds such that they do not violate these kinematic constraints. Second, we design adaptive robot controllers that stabilize the system, which has uncertain robot mass parameters, to the desired manifolds of motion. We prove that the closed-loop system will converge to the target transport speed and direction for all initial conditions that are far enough from singular configurations (described in section IV).

Although adaptive control has previously been used for cooperative manipulation in [12], [15], [16], [17], [18] these strategies require precise robot localization, predefined trajectories for each robot and/or for the payload, and knowledge about the position of the payload's center of mass and the robots' distribution around the payload. In addition, since the desired manifolds of motion are designed without accounting for the holonomic constraints between the robots and the payload, these strategies require knowledge of the position of each robot's attachment point relative to the payload's center of mass. In contrast, we design the desired manifolds of motion of the system so that they are consistent with the holonomic constraints between the robots and the payload. Moreover, our control strategy *only requires local robot measurements of their own motion*, and it does not rely on any of the information required by the aforementioned adaptive control strategies.

II. Problem Statement

We consider a team of N identical autonomous ground robots that are arranged on a planar surface in an arbitrary configuration around a payload, as in Fig. 1. Each robot is comprised of a differential-drive core module, equipped with a 1-DOF manipulator arm that can rotate about the core's central axis. We assume that the manipulator arm of each robot is attached to the load via a point grasp and that the load is lifted above the ground. We also assume that each robot can measure its own speed and heading, as well as the rotation angle and angular velocity of its manipulator. The robots do not have global localization or communication capabilities, and they lack information about the payload's physical properties, velocity, and the position of its center of mass; the number of robots in the transport team; and the robots' distribution around the payload.

Our objective is to design decentralized robot controllers that drive the team to collectively transport the load at a desired speed along a straight path in a target direction. We assume that each robot knows the target speed and direction, although they are not assigned predefined trajectories. As an extension of this approach, we note that we could design controllers that drive the payload along a predefined sequence of straight paths, each associated with a target transport speed and heading. To enable the robots to act autonomously during transport, the controllers must not depend on global feedback, which would require the presence of a central supervisor. Instead, the controllers must rely only on the minimal local information that is available to each robot.

III. Dynamical Model

To derive the equation of motion of each 3-DOF robot in the transport team, we must first choose a vector of generalized coordinates that describe the configuration of the robot, illustrated in Fig. 2. We define $\boldsymbol{x}_i = [x_i \; y_i]^T \in \mathbb{R}^2$ as the position of the center of the i^{th} robot's core in the global coordinate frame I, θ_i as its heading angle with respect to the global frame, θ_{R_i} and θ_{L_i} as the angular positions of the right and left wheels, and ϕ_i as the angular position of the manipulator with respect to a coordinate frame R that is fixed to the core. If we select $\boldsymbol{Q}_i = [x_i \; y_i \; \theta_i \; \theta_{R_i} \; \theta_{L_i} \; \phi_i]^T \in \mathbb{R}^6$ as the generalized coordinates for robot i, the dynamics of the robot must include the Lagrange multipliers that are associated with the nonholonomic constraints between the robot's translational and rotational motion. Alternatively, we can use the generalized coordinates $\boldsymbol{q}_i^* = [\theta_{R_i} \;\; \theta_{L_i} \;\; \phi_i]^T$ to formulate the dynamics of the robot in an unconstrained form, as described in Appendix I. Moreover, if we use the invertible transformation $\boldsymbol{q}_i = \boldsymbol{T}\boldsymbol{q}_i^*$ with

$$\boldsymbol{T} = \begin{bmatrix} \frac{r}{2} & \frac{r}{2} & 0 \\ \frac{r}{b} & \frac{-r}{b} & 0 \\ 0 & 0 & 1 \end{bmatrix}, \tag{1}$$

in which r is the radius of the robot's wheels and b is the distance between the wheels, then we obtain a new vector of generalized coordinates that are more suitable for our control objectives:

$$\boldsymbol{q}_i = \begin{bmatrix} \frac{r}{2}(\theta_{R_i} + \theta_{L_i}) \\ \frac{r}{b}(\theta_{R_i} - \theta_{L_i}) \\ \phi_i \end{bmatrix}. \tag{2}$$

Defining ξ_i as the length of the path traveled by the center of the i^{th} robot's core, the time derivative $\dot{\xi}_i$ is the speed of this point. From the kinematics equations for a differential-drive robot, given by Eq. (40)–Eq. (41) in Appendix I, we find that the time derivative of the first and second elements of $\boldsymbol{q}_i$ are equal to $\dot{\xi}_i$ and $\dot{\theta}_i$, respectively. Therefore,

$$\dot{\boldsymbol{q}}_i = \begin{bmatrix} \dot{\xi}_i & \dot{\theta}_i & \dot{\phi}_i \end{bmatrix}^T. \tag{3}$$

These coordinates express the motion of the robot directly in terms of the parameters that we need to control: the robot's translational motion and heading, and its manipulator arm's angular position.

While engaged in cooperative transport, the dynamics of robot i can be written in the following general form [19]:

$$\boldsymbol{M}_i(\boldsymbol{q}_i)\ddot{\boldsymbol{q}}_i + \boldsymbol{C}_i(\boldsymbol{q}_i, \dot{\boldsymbol{q}}_i)\dot{\boldsymbol{q}}_i + \boldsymbol{N}_i(\boldsymbol{q}_i, \dot{\boldsymbol{q}}_i) = \boldsymbol{\tau}_i - \boldsymbol{J}_i^T\boldsymbol{F}_i, \tag{4}$$

where $\boldsymbol{q}_i \in \mathbb{R}^3$ is the vector of generalized coordinates defined in Eq. (2), $\boldsymbol{\tau}_i \in \mathbb{R}^3$ is the vector of actuator torques, $\boldsymbol{F}_i \in \mathbb{R}^2$ is the force exerted on the robot by the payload, $\boldsymbol{J}_i \in \mathbb{R}^{2\times 3}$ is the Jacobian matrix of the end-effector's position, $\boldsymbol{M}_i \in \mathbb{R}^{3\times 3}$ is the inertia matrix, $\boldsymbol{C}_i \in \mathbb{R}^3$ is the Coriolis matrix, and $\boldsymbol{N}_i \in \mathbb{R}^3$ is a vector that includes the effect of gravity and frictional forces at the joints.

In addition, we derive the the dynamics of the payload during cooperative transport. Let m_o be the mass of the load and J_o be the load's moment of inertia about the axis

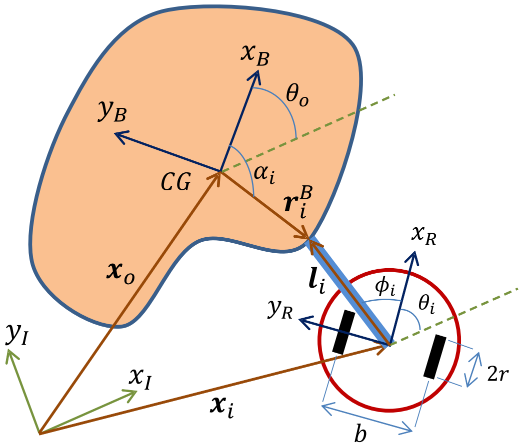

Fig. 2. A Pheeno robot in a collective transport task with the kinematic chain representing the holonomic constraint between it and the payload.

normal to the plane of the motion and passing through its center of gravity (CG). Then $\boldsymbol{M}_o = diag(m_o, m_o, J_o) \in \mathbb{R}^{3\times3}$ denotes the payload's inertia matrix. We define $\boldsymbol{q}_o = [x_o\ y_o\ \theta_o]^T \in \mathbb{R}^3$ as the payload's vector of generalized coordinates, where x_o and y_o are the position coordinates of the load's CG and θ_o is the load's heading, all with respect to the global frame I. Because there is a point grasp at each robot's attachment point to the load, there exists a kinematic chain passing through the load's CG, the attachment point, and the robot core's center, as illustrated in Fig. 2. Then we will use the *grasp matrix* [20], $\boldsymbol{G} \in \mathbb{R}^{3\times2N}$, given by:

$$\boldsymbol{G} = \begin{bmatrix} \boldsymbol{G}_1 & \cdots & \boldsymbol{G}_N \end{bmatrix}, \tag{5}$$

where

$$\boldsymbol{G}_i = \begin{bmatrix} 1 & 0 \\ 0 & 1 \\ -||\boldsymbol{r}_i^B|| \sin(\theta_o + \alpha_i) & ||\boldsymbol{r}_i^B|| \cos(\theta_o + \alpha_i) \end{bmatrix}, \tag{6}$$

in which $\boldsymbol{r}_i^B \in \mathbb{R}^2$ is the vector from the load's CG to the attachment point of robot i, and α_i is the angle of this vector with respect to the load's local coordinate system. Finally, we define $\boldsymbol{F}_i \in \mathbb{R}^2$ as the force exerted by robot i on the load, expressed in the global frame, and $\boldsymbol{F} \in \mathbb{R}^{2N}$ as the concatenation of all the robots' applied forces:

$$\boldsymbol{F} = \begin{bmatrix} \boldsymbol{F}_1^T & \cdots & \boldsymbol{F}_N^T \end{bmatrix}^T. \tag{7}$$

Then, the dynamics of the payload can be written as

$$\boldsymbol{M}_o \ddot{\boldsymbol{q}}_o = \boldsymbol{G}\boldsymbol{F}. \tag{8}$$

IV. Holonomic Constraints and Design of the Desired Manifolds of Motion

Using the notation in Fig. 2, the kinematic chain that represents the holonomic constraint between a robot and the payload can be expressed as:

$$\boldsymbol{x}_i + \boldsymbol{l}_i - \boldsymbol{R}_B^I \boldsymbol{r}_i^B - \boldsymbol{x}_o \ = \ \boldsymbol{0}, \tag{9}$$

in which $\boldsymbol{x}_i = [x_i\ y_i]^T \in \mathbb{R}^2$ is the position of the center of robot i's core in the global frame, $\boldsymbol{l}_i \in \mathbb{R}^2$ is the vector from $\boldsymbol{x}_i$ to the attachment point of robot i on the load, $\boldsymbol{R}_B^I \in \mathbb{R}^{2\times2}$ is the rotation matrix from the payload's local frame to the global frame, and $\boldsymbol{x}_o = [x_o\ y_o]^T \in \mathbb{R}^2$ is the position of the payload's CG in the global frame. Taking the time derivative of this equation, we can write it in the form of an integrable Pfaffian constraint [19],

$$\boldsymbol{A}_i(\boldsymbol{q}_i, \boldsymbol{q}_o) \begin{bmatrix} \dot{\boldsymbol{q}}_i \\ \dot{\boldsymbol{q}}_o \end{bmatrix} = \boldsymbol{0}, \tag{10}$$

where $\boldsymbol{A}_i = [\boldsymbol{J}_i \ \ -\boldsymbol{G}_i^T]$, in which

$$\boldsymbol{J}_i = \begin{bmatrix} \cos(\theta_i) & -l_i \sin(\theta_i + \phi_i) & -l_i \sin(\theta_i + \phi_i) \\ \sin(\theta_i) & l_i \cos(\theta_i + \phi_i) & l_i \cos(\theta_i + \phi_i) \end{bmatrix} \tag{11}$$

with $l_i = \|\boldsymbol{l}_i\|$, and $\boldsymbol{G}_i$ given by Eq. (6).

In the case of N robots, the constraint Eq. (9) exists between each robot and the payload. Then Eq. (10) can be expanded to include all N constraints:

$$\boldsymbol{A}(\boldsymbol{q}_a)\dot{\boldsymbol{q}}_a = \boldsymbol{0}, \tag{12}$$

where $\boldsymbol{q}_a = [\boldsymbol{q}^T \ \ {\boldsymbol{q}_o}^T]^T \in \mathbb{R}^{3N+3}$, in which $\boldsymbol{q} = [{\boldsymbol{q}_1}^T \ \cdots \ {\boldsymbol{q}_N}^T]^T \in \mathbb{R}^{3N}$, and the *constraint matrix* $\boldsymbol{A} \in \mathbb{R}^{2N\times(3N+3)}$ is given by:

$$\boldsymbol{A}(\boldsymbol{q}_a) = \begin{bmatrix} \boldsymbol{J}_1 & \boldsymbol{0}_{2\times3} & \cdots & \boldsymbol{0}_{2\times3} & -\boldsymbol{G}_1^T \\ \boldsymbol{0}_{2\times3} & \boldsymbol{J}_2 & \boldsymbol{0}_{2\times3} & \cdots & -\boldsymbol{G}_2^T \\ \vdots & \vdots & \vdots & \vdots & \vdots \\ \boldsymbol{0}_{2\times3} & \cdots & \boldsymbol{0}_{2\times3} & \boldsymbol{J}_N & -\boldsymbol{G}_N^T \end{bmatrix}. \tag{13}$$

Eq. (12) describes the allowable velocities of the system in the entire configuration space. This means that these velocities can evolve only in the null space of $\boldsymbol{A}$, and we must take this fact into account when designing the desired manifolds of motion. Otherwise, the desired system behavior, which is described by the manifolds, would not be reachable by trajectories of the system.

We aim to design robot controllers that do not require any information about the payload's position and velocity and the distribution of robots around the payload. Toward this end, we design the desired manifold of motion for a single robot i by considering its constraint with the payload, defined by the matrix $\boldsymbol{A}_i$, and then showing that the manifolds for all N robots are compatible with the entire set of N constraints, defined by the matrix $\boldsymbol{A}$.

For mechanical systems, any first-order desired manifold of motion can be written in the general form $\boldsymbol{\psi} = \dot{\boldsymbol{\eta}} - \dot{\boldsymbol{\eta}}_r$, where $\dot{\boldsymbol{\eta}}$ is the vector of system velocities and $\dot{\boldsymbol{\eta}}_r$ is the vector of reference velocities, which can be a function of time and $\boldsymbol{\eta}$ [21]. In general, $\boldsymbol{\psi}$ must be driven to zero, at which point $\dot{\boldsymbol{\eta}}$ will track $\dot{\boldsymbol{\eta}}_r$. Here, defining $\boldsymbol{\eta}_i := [\boldsymbol{q}_i^T \ \boldsymbol{q}_o^T]^T \in \mathbb{R}^6$ as the vector of the generalized coordinates of robot i and the payload, we specify a reference velocity vector $\dot{\boldsymbol{\eta}}_{r_i} := [\dot{\boldsymbol{q}}_{r_i}^T \ \dot{\boldsymbol{q}}_{r_o}^T]^T \in \mathbb{R}^6$ that lies in the null space of $\boldsymbol{A}_i$ so that it is achievable by $\dot{\boldsymbol{\eta}}_i$. The null space of $\boldsymbol{A}_i$ can be written as:

$$\mathcal{N}(\boldsymbol{A}_i) = span(\boldsymbol{e}_{1_i},\ \boldsymbol{e}_{2_i},\ \boldsymbol{e}_{3_i},\ \boldsymbol{e}_{4_i}), \tag{14}$$

where

$$\boldsymbol{e}_{1_i} = [\,0\ \ -1\ 1\ 0\ 0\ 0\,]^T\ ,$$
$$\boldsymbol{e}_{2_i} = \left[\ \frac{\cos(\theta_i+\phi_i)}{\cos(\phi_i)}\ \ \frac{-\sin(\theta_i)}{l_i\cos(\phi_i)}\ \ 0\ 1\ 0\ 0\ \right]^T\ ,$$
$$\boldsymbol{e}_{3_i} = \left[\ \frac{\sin(\theta_i+\phi_i)}{\cos(\phi_i)}\ \ \frac{\cos(\theta_i)}{l_i\cos(\phi_i)}\ \ 0\ 0\ 1\ 0\ \right]^T\ ,$$
$$\boldsymbol{e}_{4_i} = [\,e_{41_i}\ e_{42_i}\ 0\ 0\ 0\ 1\,]^T\ , \tag{15}$$

in which the first two elements of the vector $\boldsymbol{e}_{4_i}$ are:

$$e_{41_i} = \frac{-||\boldsymbol{r}_i^B||\sin(\theta_o+\alpha_i-\theta_i-\phi_i)}{\cos(\phi_i)},$$
$$e_{42_i} = \frac{||\boldsymbol{r}_i^B||\cos(\theta_o+\alpha_i-\theta_i-\phi_i)}{\cos(\phi_i)}. \tag{16}$$

Indeed, the vector $\dot{\boldsymbol{\eta}}_{r_i}$ must be a linear combination of these four vectors, since they span $\mathcal{N}(\boldsymbol{A}_i)$. As stated in section II, the desired motion for the payload is a regulated speed along the x_I direction, zero speed along the y_I direction, and zero angular speed. Thus, we set:

$$\dot{\boldsymbol{q}}_{r_o} = [v_{des}\ 0\ 0]^T, \tag{17}$$

where v_{des} is the desired speed of transport. Then, noting the 1's in the fifth and sixth elements of $\boldsymbol{e}_{3_i}$ and $\boldsymbol{e}_{4_i}$, respectively, we can conclude that $\dot{\boldsymbol{\eta}}_{r_i}$ cannot have any projection on these two vectors and must be a linear combination of only $\boldsymbol{e}_{1_i}$ and $\boldsymbol{e}_{2_i}$. Moreover, the desired motion for the robot includes a regulated forward speed and a zero heading angle, in addition to a zero angular speed for the manipulator.

Here, we design the desired manifolds in a way that is applicable to general initial configurations of robots, in which the robots have an arbitrary distribution around the payload and arbitrary headings and manipulator angles, as depicted in Fig. 1. However, we must first take into account the fact that both $\boldsymbol{e}_{2_i}$ and $\boldsymbol{e}_{3_i}$ have entries with $\cos(\phi_i)$ in the denominator, and hence $\phi_i = k\pi/2$ for any integer k is a singular configuration that has to be avoided. Therefore, we consider the following assumption, which can be enforced by restricting the range of rotation of the manipulator arm (for example, $\phi_i \in 0.9[-\pi/2, \pi/2]$):

Assumption IV.1. *Each robot starts the transport from a configuration far from singular configurations, and stays far from these configurations during the entire transport.*

The reference velocity vector is specified as

$$\dot{\boldsymbol{\eta}}_{r_i} \ = \ v_{des}\boldsymbol{e}_{2_i}, \tag{18}$$

and therefore, the desired manifold of motion is given by

$$\boldsymbol{\psi}_i = \dot{\boldsymbol{\eta}}_i - \dot{\boldsymbol{\eta}}_{r_i}. \tag{19}$$

This manifold can be written as $\boldsymbol{\psi}_i = [\boldsymbol{s}_i^T\ \boldsymbol{s}_o^T]^T$, where $\boldsymbol{s}_i$ and $\boldsymbol{s}_o$ are the desired manifolds for robot i and the payload, respectively:

$$\boldsymbol{s}_i = \begin{bmatrix} \dot{\xi}_i - v_{des}\frac{\cos(\theta_i+\phi_i)}{\cos(\phi_i)} \\ \dot{\theta}_i + v_{des}\frac{\sin(\theta_i)}{l_i\cos(\phi_i)} \\ \dot{\phi}_i \end{bmatrix},\ \ \boldsymbol{s}_o = \begin{bmatrix} \dot{x}_o - v_{des} \\ \dot{y}_o \\ \dot{\theta}_o \end{bmatrix}. \tag{20}$$

We see that $\boldsymbol{s}_o$ is independent of the robot's state variables. We now show that the reference velocity vector Eq. (18) is compatible with all holonomic constraints in the system, *i.e.* Eq. (12), and then we prove that it produces the desired motion characteristics of the payload and the robots.

Proposition IV.2. *The desired velocities in Eq. (18) are reachable by all robots in the team and the payload during collective transport.*

Proof. Since both $\dot{\boldsymbol{\eta}}_i$ and $\dot{\boldsymbol{\eta}}_{r_i}$ are in $\mathcal{N}(\boldsymbol{A}_i)$ for each robot $i = 1, ..., N$, we can conclude that $\boldsymbol{A}_i\boldsymbol{\psi}_i = \boldsymbol{0}$, $i = 1, ..., N$, which implies that

$$\begin{bmatrix}\boldsymbol{J}_i & -\boldsymbol{G}_i^T\end{bmatrix}\begin{bmatrix}\boldsymbol{s}_i \\ \boldsymbol{s}_o\end{bmatrix} = \boldsymbol{0}, \quad i = 1, ..., N. \tag{21}$$

Defining $\boldsymbol{s} := [\boldsymbol{s}_1{}^T\ \cdots\ \boldsymbol{s}_N{}^T]^T$ and $\boldsymbol{s}_a := [\boldsymbol{s}^T\ \boldsymbol{s}_o{}^T]^T$, we can rewrite the N equations in Eq. (21) in the following compact form:

$$\boldsymbol{A}(\boldsymbol{q}_a)\boldsymbol{s}_a = \boldsymbol{0}, \tag{22}$$

which means that $\boldsymbol{s}_a \in \mathcal{N}(\boldsymbol{A})$. Since the designed manifold $\boldsymbol{s}_a$ therefore satisfies the constraint Eq. (12), the reference velocity vector $\dot{\boldsymbol{\eta}}_{r_i}$ is reachable by each robot i.

□

Proposition IV.3. *On the manifolds $\boldsymbol{\psi}_i$ defined by Eq. (19), the payload's motion converges to a pure translation along the x_I direction with speed v_{des}; the robots' speeds and headings converge to v_{des} and 0, respectively; and the robots' manipulators converge to a stationary configuration.*

Proof. At the time when $\boldsymbol{\psi}_i = \boldsymbol{0}$, we have $\dot{\theta}_o = 0$, which means that the payload has stopped rotating, and $\dot{y}_o = 0$, $\dot{x}_o = v_{des}$, which means that the payload is moving along the x_I direction at the desired speed. In addition, from the elements of $\boldsymbol{s}_i$, we have that $\dot{\phi}_i = 0 \ \rightarrow \ \phi_i = const. := \phi_{i_{ss}}$, which means that the manipulator of robot i has stopped rotating. Consequently, we can conclude that $\cos(\phi_i) = const. = \cos(\phi_{i_{ss}})$, and thus the second element of $\boldsymbol{s}_i$, which governs the dynamics of the robot's heading, can be written in the following form:

$$\dot{\theta}_i + c_i\sin(\theta_i) = 0, \tag{23}$$

where $c_i = \frac{v_{des}}{l_i\cos(\phi_{i_{ss}})}$ is constant and positive for $\phi_i \in (-\pi/2, \pi/2)$, which is the manipulator's range of motion. We can show that θ_i asymptotically converges to zero as follows. We consider the following Lyapunov function W and its time derivative along the trajectories of Eq. (23):

$$W = 1 - \cos(\theta_i) \quad \rightarrow \quad \dot{W} = -c_i\sin(\theta_i)^2. \tag{24}$$

Since $\dot{W}$ is negative definite, Eq. (23) is asymptotically stable at $\theta_i = 0$, which means that robot i will converge to the desired heading.[1] Finally, since $\boldsymbol{s}_i = \boldsymbol{0}$ and θ_i converges to

[1] To keep $\theta_i(t) \in (-\pi, \pi)$, the robot moves backward when the absolute value of its initial heading error is more than $\pi/2$. This is implemented by switching the desired speed to $-v_{des}$ and shifting the desired heading by $-\pi$ rad.

zero, we can write the following for the first element of $\boldsymbol{s}_i$:

$$\lim_{t\to\infty} \dot{\xi}_i = v_{des} \lim_{\theta_i \to 0} \frac{\cos(\theta_i + \phi_{i_{ss}})}{\cos(\phi_{i_{ss}})} = v_{des}, \tag{25}$$

which shows that the robot's speed will converge to the desired value. $\square$

Remark IV.4. *The compatibility of the desired manifolds of motion in Eq. (19) with the holonomic constraints between the robots and the payload enables the robots to perform the transport task without information about the position of the payload's center of mass or the vector from this point to each robot's attachment point, i.e.* $\boldsymbol{r}_i^B$*. This information is required in many collective transport methods that have been proposed in the literature, as described in section I.*

V. Controller Design and Stability Analysis

As discussed in section IV, the desired system behavior is achieved on the manifolds expressed as $\boldsymbol{\psi}_i = [\boldsymbol{s}_i^T \ \boldsymbol{s}_o^T]^T$, in which $\boldsymbol{s}_i := [s_{\xi_i} \ s_{\theta_i} \ s_{\phi_i}]^T$ is associated with the dynamics of robot i, and $\boldsymbol{s}_o$ is associated with the payload's dynamics. Moreover, it is possible to verify that the terms $\boldsymbol{M}_i(\boldsymbol{q}_i)$, $\boldsymbol{C}_i(\boldsymbol{q}_i, \dot{\boldsymbol{q}}_i)$, and $\boldsymbol{N}_i(\boldsymbol{q}_i, \dot{\boldsymbol{q}}_i)$ in Eq. (4) can be linearly parametrized in terms of a constant vector $\boldsymbol{\Theta}_i \in \mathbb{R}^P$ that contains P uncertain mass and geometric properties of robot i [21]. Thus, we can define a matrix $\boldsymbol{Y}_i = \boldsymbol{Y}_i(\boldsymbol{q}_i, \dot{\boldsymbol{q}}_i, \dot{\boldsymbol{q}}_{r_i}, \ddot{\boldsymbol{q}}_{r_i}) \in \mathbb{R}^{3\times P}$, which is a function of the reference quantities $\dot{\boldsymbol{q}}_{r_i}, \ddot{\boldsymbol{q}}_{r_i}$ and the measured quantities $\boldsymbol{q}_i, \dot{\boldsymbol{q}}_i$, such that:

$$\begin{aligned} \boldsymbol{M}_i(\boldsymbol{q}_i)\ddot{\boldsymbol{q}}_{r_i} + \boldsymbol{C}_i(\boldsymbol{q}_i, \dot{\boldsymbol{q}}_i)\dot{\boldsymbol{q}}_{r_i} + \boldsymbol{N}_i(\boldsymbol{q}_i, \dot{\boldsymbol{q}}_i) = \\ \boldsymbol{Y}_i(\boldsymbol{q}_i, \dot{\boldsymbol{q}}_i, \dot{\boldsymbol{q}}_{r_i}, \ddot{\boldsymbol{q}}_{r_i})\boldsymbol{\Theta}_i. \end{aligned} \tag{26}$$

Here, we assume that we have uncertain estimates of $P = 3$ parameters for each robot: the mass and moment of inertia of its core, and the mass of its manipulator.

We now design the controller for the actuator torque that is applied by the wheels and manipulator of robot i. This torque is defined as $\boldsymbol{\tau}_i^* = \boldsymbol{T}^{-1}\boldsymbol{\tau}_i$, where

$$\boldsymbol{\tau}_i = -\boldsymbol{K}\boldsymbol{s}_i + \boldsymbol{Y}_i\hat{\boldsymbol{\Theta}}_i. \tag{27}$$

Here, $\boldsymbol{K} \in \mathbb{R}^{3\times 3}$ is a positive definite matrix that contains the controller gains, and $\hat{\boldsymbol{\Theta}}_i$ is an estimate of $\boldsymbol{\Theta}_i$, which is updated according to the following adaptation law:

$$\dot{\hat{\boldsymbol{\Theta}}}_i = -\boldsymbol{\Gamma}\boldsymbol{Y}_i^T\boldsymbol{s}_i, \tag{28}$$

in which $\boldsymbol{\Gamma} \in \mathbb{R}^{3\times 3}$ is a symmetric positive definite matrix that contains the adaptation gains.

Remark V.1. *The controller in Eq. (27) and the adaptation law in Eq. (28) are completely decentralized, in the sense that each robot i can execute them using only measurements of its own motion (i.e., the quantities in $\boldsymbol{s}_i$ and $\boldsymbol{Y}_i$). They also do not require any information about the payload's motion and the robots' distribution around the payload.*

To ensure that the controller in Eq. (27) and the adaptation law in Eq. (28) drive the system trajectories to the desired manifolds, we prove the stability of the closed-loop system in Theorem V.3. First, we state the following lemma, which will be used in the proof of the theorem.

Lemma V.2. *Consider a team of $N \geq 2$ robots that are attached to a payload at distinct points, with the robots' reference velocities specified as in Eq. (18). If $\boldsymbol{s}_i \equiv \boldsymbol{0}$ for each robot $i \in \{1, 2, ..., N\}$, then $\boldsymbol{s}_o \equiv \boldsymbol{0}$.*

Proof. Since both $\dot{\boldsymbol{q}}_a$ and $\dot{\boldsymbol{q}}_{a_r}$ are in $\mathcal{N}(\boldsymbol{A})$, we can write $\boldsymbol{A}\boldsymbol{s}_a = \boldsymbol{0}$. Thus, according to Eq. (12), we have:

$$\boldsymbol{J}\boldsymbol{s} = \boldsymbol{G}^T\boldsymbol{s}_o, \tag{29}$$

in which $\boldsymbol{J} \in \mathbb{R}^{2N\times 3N}$ is a rectangular matrix in block-diagonal form, with the blocks defined as $\boldsymbol{J}_i$, $i = 1, ..., N$. When $\boldsymbol{s}_i = \boldsymbol{0}$ for all $i = 1, ..., N$, then $\boldsymbol{s} = \boldsymbol{0}$. This implies that $\boldsymbol{J}\boldsymbol{s} = \boldsymbol{0}$, which means that $\boldsymbol{G}^T\boldsymbol{s}_o = \boldsymbol{0}$. Moreover, $\boldsymbol{G} \in \mathbb{R}^{3\times 2N}$, and its first two rows, which are the first two columns of $\boldsymbol{G}^T$, are linearly independent. The third row is linearly dependent on the other rows only in the case where $||\boldsymbol{r}_i^B|| \sin(\theta_o + \alpha_i) = ||\boldsymbol{r}_j^B|| \sin(\theta_o + \alpha_j)$ and $||\boldsymbol{r}_i^B|| \cos(\theta_o + \alpha_i) = ||\boldsymbol{r}_j^B|| \cos(\theta_o + \alpha_j)$ $\forall\ i, j \in \{1, 2, ..., N\}$, which is impossible because the robots are attached to distinct points on the payload. Therefore, all columns of $\boldsymbol{G}^T$ are linearly independent, and so $rank(\boldsymbol{G}^T) = 3$, which implies that $dim(\boldsymbol{\mathcal{N}}(\boldsymbol{G}^T)) = 3 - 3 = 0$. Hence, the null space of $\boldsymbol{G}^T$ is empty, and the only solution for $\boldsymbol{G}^T\boldsymbol{s}_o = \boldsymbol{0}$ is $\boldsymbol{s}_o \equiv \boldsymbol{0}$. $\square$

Theorem V.3. *Consider a team of N differential-drive robots, each with a 1-DOF manipulator arm that is attached to a payload via a point grasp, as depicted in Fig. 1. Given the manifold in Eq. (20) and the controller and adaptation law in Eq. (27) and Eq. (28), the entire system converges to the desired motion, which is defined as the translation of the payload and robots in a specified direction at a target speed without rotation, with the robots' manipulators fixed in a stationary configuration.*

Proof. We consider the following Lyapunov function [21]:

$$V = \frac{1}{2}\sum_{i=1}^{N} \boldsymbol{s}_i^T\boldsymbol{M}_i\boldsymbol{s}_i + \frac{1}{2}\boldsymbol{s}_o^T\boldsymbol{M}_o\boldsymbol{s}_o + \frac{1}{2}\sum_{i=1}^{N} \tilde{\boldsymbol{\Theta}}_i^T\boldsymbol{\Gamma}^{-1}\tilde{\boldsymbol{\Theta}}_i, \tag{30}$$

in which $\tilde{\boldsymbol{\Theta}}_i = \hat{\boldsymbol{\Theta}}_i - \boldsymbol{\Theta}_i$ is the parameter estimation error. The time derivative of this function is:

$$\begin{aligned} \dot{V} = & \sum_{i=1}^{N} \boldsymbol{s}_i^T\boldsymbol{M}_i\dot{\boldsymbol{s}}_i + \frac{1}{2}\sum_{i=1}^{N} \boldsymbol{s}_i^T\dot{\boldsymbol{M}}_i\boldsymbol{s}_i \\ & + \boldsymbol{s}_o^T\boldsymbol{M}_o\dot{\boldsymbol{s}}_o + \frac{1}{2}\boldsymbol{s}_o^T\dot{\boldsymbol{M}}_o\boldsymbol{s}_o + \sum_{i=1}^{N} \dot{\tilde{\boldsymbol{\Theta}}}_i^T\boldsymbol{\Gamma}^{-1}\tilde{\boldsymbol{\Theta}}_i. \end{aligned} \tag{31}$$

Since $\boldsymbol{M}_o$ is constant, and by Eq. (17), $\ddot{\boldsymbol{q}}_{r_o}$, which is included in $\dot{\boldsymbol{s}}_o$, is equal to zero, $\dot{V}$ is reduced to:

$$\begin{aligned} \dot{V} = & \sum_{i=1}^{N} \boldsymbol{s}_i^T\boldsymbol{M}_i(\ddot{\boldsymbol{q}}_i - \ddot{\boldsymbol{q}}_{r_i}) + \frac{1}{2}\sum_{i=1}^{N} \boldsymbol{s}_i^T\dot{\boldsymbol{M}}_i\boldsymbol{s}_i \\ & + \boldsymbol{s}_o^T\boldsymbol{M}_o\ddot{\boldsymbol{q}}_o + \sum_{i=1}^{N} \dot{\tilde{\boldsymbol{\Theta}}}_i^T\boldsymbol{\Gamma}^{-1}\tilde{\boldsymbol{\Theta}}_i. \end{aligned} \tag{32}$$

Furthermore, considering the passivity property of the robot dynamics in Eq. (4) [19], recognizing that the matrix $\dot{\boldsymbol{M}}_i - 2\boldsymbol{C}_i$ is skew-symmetric, noting the payload's dynamics in Eq. (8), and substituting the controller Eq. (27) into the expression for $\boldsymbol{M}_i\ddot{\boldsymbol{q}}_i$ from Eq. (4), $\dot{V}$ can be rewritten as:

$$\begin{aligned}\dot{V} = &-\sum_{i=1}^{N} \boldsymbol{s}_i^T \boldsymbol{K} \boldsymbol{s}_i + \sum_{i=1}^{N} \boldsymbol{s}_i^T \boldsymbol{Y}_i \hat{\boldsymbol{\Theta}}_i \\ &- \sum_{i=1}^{N} \boldsymbol{s}_i^T \left(\boldsymbol{M}_i(\boldsymbol{q}_i)\ddot{\boldsymbol{q}}_{r_i} + \boldsymbol{C}_i(\boldsymbol{q}_i, \dot{\boldsymbol{q}}_i)\dot{\boldsymbol{q}}_{r_i} + \boldsymbol{N}_i(\boldsymbol{q}_i, \dot{\boldsymbol{q}}_i)\right) \\ &+ \sum_{i=1}^{N} \dot{\tilde{\boldsymbol{\Theta}}}_i^T \boldsymbol{\Gamma}^{-1} \tilde{\boldsymbol{\Theta}}_i - \begin{bmatrix} \boldsymbol{s}^T & \boldsymbol{s}_o^T \end{bmatrix} \begin{bmatrix} \boldsymbol{J}^T \\ -\boldsymbol{G} \end{bmatrix} \boldsymbol{F}. \end{aligned} \quad (33)$$

From Eq. (13), the last term on the right-hand side of Eq. (33) can be rewritten as $(\boldsymbol{A}\boldsymbol{s}_a)^T\boldsymbol{F}$, and invoking Eq. (22), we conclude that this term is zero. Finally, applying the linear parameterization in Eq. (26) and the adaptation law in Eq. (28), and also using the fact that $\dot{\tilde{\boldsymbol{\Theta}}}_i = \dot{\hat{\boldsymbol{\Theta}}}_i$ since $\boldsymbol{\Theta}_i$ is constant, we have:

$$\dot{V} = -\sum_{i=1}^{N} \boldsymbol{s}_i^T \boldsymbol{K} \boldsymbol{s}_i. \quad (34)$$

The negative semi-definiteness of $\dot{V}$ implies the global stability of the system and, consequently, the boundedness of $\boldsymbol{s}_o$, $\boldsymbol{s}_i$, and $\tilde{\boldsymbol{\Theta}}_i$ for all $i = 1, ..., N$. From Eq. (27), this result implies the boundedness of each $\boldsymbol{\tau}_i$. By eliminating the vector $\boldsymbol{F}$ from the dynamics of the N robots (Eq. (4)) and the payload (Eq. (8)), we observe that $\boldsymbol{\tau}_i$, $i = 1, ..., N$, are the only active torques affecting the dynamics of the entire system of the robots and payload. Since these torques are bounded, we can conclude that $\dot{\boldsymbol{q}}_i$ and $\ddot{\boldsymbol{q}}_i$ are bounded for each robot i. The boundedness of $\ddot{\boldsymbol{q}}_{r_i}$ can be verified from Eq. (20). Since $\ddot{\boldsymbol{q}}_i$ and $\ddot{\boldsymbol{q}}_{r_i}$ are both bounded, we have that $\dot{\boldsymbol{s}}_i = \ddot{\boldsymbol{q}}_i - \ddot{\boldsymbol{q}}_{r_i}$ is also bounded. Furthermore, the second time derivative of V can be calculated as:

$$\ddot{V} = -2\sum_{i=1}^{N} \boldsymbol{s}_i^T \boldsymbol{K} \dot{\boldsymbol{s}}_i. \quad (35)$$

Given that $\boldsymbol{s}_i$ and $\dot{\boldsymbol{s}}_i$ are bounded for all i as discussed above, this equation indicates that $\ddot{V}$ is bounded as well. By *Barbalat's lemma* [21], the positive definiteness of V and the boundedness of $\ddot{V}$ imply that $\dot{V} \to 0$, and consequently $\boldsymbol{s}_i \to 0$, as $t \to \infty$. Finally, from Lemma V.2, we conclude that $\boldsymbol{s}_o \to 0$ as $t \to \infty$, which completes the proof. □

Proposition V.4. *All internal forces $\boldsymbol{F}_i$, which are exerted by the robots on the payload, remain bounded during transport.*

Proof. In the proof of Theorem V.3, we showed that $\dot{\boldsymbol{q}}_i$, $\ddot{\boldsymbol{q}}_i$, and $\boldsymbol{\tau}_i$ are all bounded. We can then conclude from the robot equations of motion (4) that the term $\boldsymbol{J}_i^T\boldsymbol{F}_i$ is also bounded for each robot i. In addition, we can confirm that the null space of $\boldsymbol{J}_i^T$ is empty. This implies that all internal forces $\boldsymbol{F}_i$ remain bounded as well. □

VI. Simulation Results

We validated our adaptive control strategy with high-fidelity 3D physics simulations in the robot simulator Webots [22]. The robots in the Webots simulations are 3D models of a small mobile robot platform, *Pheeno*, that has been developed in our lab [1].

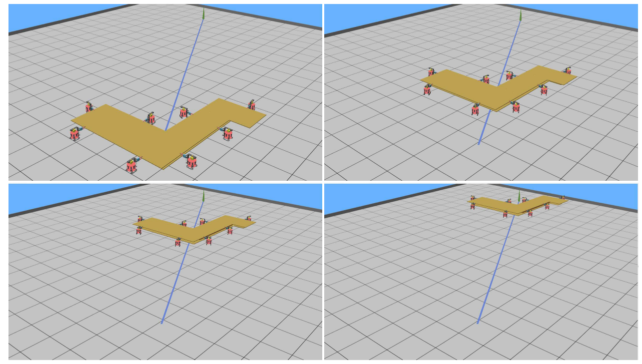

Fig. 3. Collective transport by eight Pheenos simulated in Webots.

We implemented the controller and adaptation law proposed in section V in a Webots simulation in which eight Pheeno robots transport the payload to a goal that is located at a heading of $\gamma = 30°$ in the inertial frame. The desired load speed is $v_{des} = 0.2$ m/s, and the load mass and moment of inertia are 1 kg and 0.33 kg·m^2, respectively. The matrices of controller and adaptation gains were set to $\boldsymbol{K} = diag(0.002, 0.006, 0.01)$ and $\boldsymbol{\Gamma} = diag(0.3, 0.5, 0.2)$. The system was simulated for 150 s.

Four snapshots of the simulation are shown in Fig. 3, in which the goal location is indicated by the green cone and the desired path of the payload's CG is illustrated by the blue line. Fig. 4 plots the load and robot trajectories, which are straight and parallel in the desired direction without significant rotation for the load.

Fig. 5 displays the time evolution of the entries of the desired manifold $\boldsymbol{s}_i$ for each robot i (here we drop the i subscripts for simplicity): s_ξ, s_θ, and s_ϕ, which are associated with the robot's speed $\dot{\xi}$, heading angle θ, and manipulator angle ϕ, respectively. The figure also plots the time evolution of $\dot{\xi}$, θ, and ϕ for each robot. The variables are only plotted over the beginning of the simulation in order to clearly illustrate their transient dynamics. The plots show that s_ξ, s_θ, and s_ϕ all converge to zero for each robot, and although they initially exhibit oscillations, they have smooth profiles after $\sim$ 6 s. The manipulator angles of the robots all converge to steady-state values, demonstrating that each robot converges to a fixed configuration. Note that these angles remain far from the singular configuration, *i.e.* $\pm 90°$, in accordance with Assumption IV.1. Furthermore, four of the robots, which push the payload, converge to a heading of 30° and speed of 0.2 m/s, while the other four robots, which pull the payload, converge to a heading of $-150°$ and speed of -0.2 m/s. This discrepancy in heading and speed between the pushing and pulling robots happens due to the maneuver described in the footnote in section IV. This maneuver prevents the robots from performing unnecessarily large rotations that would slow down their response and possibly drive them to singular configurations.

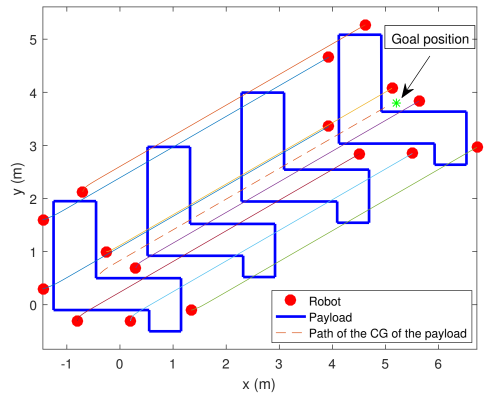

Fig. 4. The trajectories of the Pheenos and the load during transport.

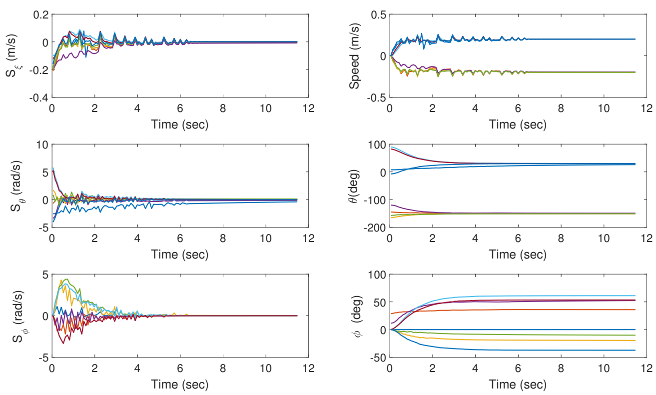

Fig. 5. Time evolution of variables in the Webots simulation of collective transport. *Left column:* Entries of the desired manifold $\boldsymbol{s}_i$ for each robot i: s_ξ, s_θ, and s_ϕ (we drop the i subscripts for simplicity). *Right column:* Speed $\dot{\xi}$, heading angle θ, and manipulator angle ϕ of each robot.

VII. Conclusion and Future Work

In this paper, we presented a decentralized adaptive control strategy for multi-robot collective transport. The controllers do not require inter-robot communication, information about the payload dynamics and geometry, or knowledge of the number of robots in the transport team and their distribution around the payload. In addition, since the desired manifolds of motion are designed to be consistent with the system's holonomic constraints, the robots are not required to begin the transport task in any specific configuration. In future work, we will consider transport teams in which the robots have manipulators with more degrees of freedom, and we will modify our controller to achieve internal force regulation and payload transport along curved reference trajectories.

References

[1] S. Wilson, R. Gameros, M. Sheely, M. Lin, K. Dover, R. Gevorkyan, M. Haberland, A. Bertozzi, and S. Berman, "Pheeno, a versatile swarm robotic research and education platform," *IEEE Robotics and Automation Letters*, vol. 1, no. 2, pp. 884–891, 2016.

[2] Z. Wang and M. Schwager, "Force-amplifying n-robot transport system (force-ants) for cooperative planar manipulation without communication," *The International Journal of Robotics Research*, vol. 35, no. 13, pp. 1564–1586, 2016.

[3] A. Yufka and M. Ozkan, "Formation-based control scheme for cooperative transportation by multiple mobile robots," *International Journal of Advanced Robotic Systems*, vol. 12, no. 9, p. 120, 2015.

[4] A. Tsiamis, C. K. Verginis, C. P. Bechlioulis, and K. J. Kyriakopoulos, "Cooperative manipulation exploiting only implicit communication," in *IEEE/RSJ International Conference on Intelligent Robots and Systems (IROS)*. IEEE, 2015, pp. 864–869.

[5] J. Chen, M. Gauci, W. Li, A. Kolling, and R. Groß, "Occlusion-based cooperative transport with a swarm of miniature mobile robots," *IEEE Transactions on Robotics*, vol. 31, no. 2, pp. 307–321, 2015.

[6] H. Bai and J. T. Wen, "Motion coordination through cooperative payload transport," in *Proc. American Control Conference (ACC)*, 2009, pp. 1310–1315.

[7] ——, "Cooperative load transport: A formation-control perspective." *IEEE Transactions on Robotics*, vol. 26, no. 4, pp. 742–750, 2010.

[8] A. Z. Bais, S. Erhart, L. Zaccarian, and S. Hirche, "Dynamic load distribution in cooperative manipulation tasks," in *IEEE/RSJ International Conference on Intelligent Robots and Systems (IROS)*. IEEE, 2015, pp. 2380–2385.

[9] S. Wilson, A. Buffin, S. C. Pratt, and S. Berman, "Multi-robot replication of ant collective towing behaviours," *Royal Society open science*, vol. 5, no. 10, p. 180409, 2018.

[10] S. Wilson, T. P. Pavlic, G. P. Kumar, A. Buffin, S. C. Pratt, and S. Berman, "Design of ant-inspired stochastic control policies for collective transport by robotic swarms," *Swarm Intelligence*, vol. 8, no. 4, pp. 303–327, 2014.

[11] M. Rubenstein, A. Cabrera, J. Werfel, G. Habibi, J. McLurkin, and R. Nagpal, "Collective transport of complex objects by simple robots: Theory and experiments," in *Proc. Int'l. Conf. on Autonomous Agents and Multi-Agent Systems (AAMAS)*, 2013, pp. 47–54.

[12] H. Lee, H. Kim, and H. J. Kim, "Planning and control for collision-free cooperative aerial transportation," *IEEE Transactions on Automation Science and Engineering*, vol. PP, no. 99, pp. 1–13, 2016.

[13] H. Farivarnejad, S. Wilson, and S. Berman, "Decentralized sliding mode control for autonomous collective transport by multi-robot systems," in *2016 IEEE 55th Conference on Decision and Control (CDC)*, Dec 2016, pp. 1826–1833.

[14] H. Farivarnejad and S. Berman, "Stability and convergence analysis of a decentralized proportional-integral control strategy for collective transport," in *2018 Annual American Control Conference (ACC)*, June 2018, pp. 2794–2801.

[15] P. Culbertson and M. Schwager, "Decentralized adaptive control for collaborative manipulation," in *Proc. IEEE International Conference on Robotics and Automation (ICRA)*, May 2018.

[16] C.-Y. Su, T.-P. Leung, and Q.-J. Zhou, "Force/motion control of constrained robots using sliding mode," *IEEE Transactions on Automatic Control*, vol. 37, no. 5, pp. 668–672, 1992.

[17] C.-Y. Su and Y. Stepanenko, "Adaptive sliding mode coordinated control of multiple robot arms attached to a constrained object," *IEEE Transactions on Systems, Man, and Cybernetics*, vol. 25, no. 5, pp. 871–878, 1995.

[18] H. Kawasaki, S. Ueki, and S. Ito, "Decentralized adaptive coordinated control of multiple robot arms without using a force sensor," *Automatica*, vol. 42, no. 3, pp. 481–488, 2006.

[19] R. M. Murray, S. S. Sastry, and L. Zexiang, *A Mathematical Introduction to Robotic Manipulation*, 1st ed. Boca Raton, FL, USA: CRC Press, Inc., 1994.

[20] S. Erhart and S. Hirche, "Model and analysis of the interaction dynamics in cooperative manipulation tasks," *IEEE Transactions on Robotics*, vol. 32, no. 3, pp. 672–683, 2016.

[21] J.-J. E. Slotine and W. Li, *Applied Nonlinear Control*. Englewood Cliffs, N.J.: Prentice Hall, 1991.

[22] O. Michel, "Webots: Professional mobile robot simulation," *International Journal of Advanced Robotic Systems*, vol. 1, no. 1, pp. 39–42, Mar. 2004.

[23] A. M. Bloch *et al.*, *Nonholonomic mechanics and control*. Springer, 2003.

Appendix I
Unconstrained Dynamics of a Nonholonomic Robot

Here, we derive the unconstrained dynamical model of a nonholonomic robot. Using the classical Lagrange formulation, we first obtain the constrained dynamics of the robot, and then eliminate the Lagrange multipliers in this constrained model. For simplicity, we drop the subscript i in the variables associated with the robot. We begin with the vector of generalized coordinates $\boldsymbol{q}_c := [x \;\; y \;\; \theta \;\; \theta_R \;\; \theta_L]^T \in \mathbb{R}^5$, which completely describes the position of each point on the robot's core as it moves. We define m_c as the mass of the robot's core, I_c as the robot core's moment of inertia about the axis that passes through its center of mass and is normal to the plane of motion, and J_w as the moment of inertia of each wheel about its axis of rotation. Hence, the Lagrangian of the robot's core is written as:

$$\mathcal{L} = \frac{1}{2}m_c(\dot{x}^2 + \dot{y}^2) + \frac{1}{2}I_c\dot{\theta}^2 + \frac{1}{2}(J_w\dot{\theta}_R^2 + J_w\dot{\theta}_L^2). \quad (36)$$

Furthermore, to satisfy the rolling condition for each wheel, we include four constraint equations that can be written in the following matrix form:

$$\boldsymbol{A}_c\dot{\boldsymbol{q}}_c = \boldsymbol{0}, \quad (37)$$

where $\boldsymbol{A}_c \in \mathbb{R}^{4\times 5}$ is

$$\boldsymbol{A}_c = \begin{bmatrix} 1 & 0 & b\cos(\theta) & -r\cos(\theta) & 0 \\ 0 & 1 & b\sin(\theta) & -r\sin(\theta) & 0 \\ 1 & 0 & -b\cos(\theta) & 0 & -r\cos(\theta) \\ 0 & 1 & -b\sin(\theta) & 0 & -r\sin(\theta) \end{bmatrix}. \quad (38)$$

Defining $\boldsymbol{\lambda} := [\lambda_1 \;\; \lambda_2 \;\; \lambda_3 \;\; \lambda_4]^T \in \mathbb{R}^4$ as the vector of Lagrange multipliers, and using the Lagrange formulation, the equations of motion of the robot's core are calculated as:

$$\begin{aligned} &m_c\ddot{x} = \lambda_1 + \lambda_3 \\ &m_c\ddot{y} = \lambda_2 + \lambda_4 \\ &I_c\ddot{\theta} = \lambda_1 b\cos(\theta) + \lambda_2 b\sin(\theta) - \lambda_3 b\cos(\theta) - \lambda_4 b\sin(\theta) \\ &J_w\ddot{\theta}_R = \tau_R - \lambda_1 r\cos(\theta) - \lambda_2 r\sin(\theta) \\ &J_w\ddot{\theta}_L = \tau_L - \lambda_3 r\cos(\theta) - \lambda_4 r\sin(\theta), \end{aligned} \quad (39)$$

where τ_R and τ_L are the actuation torques on the right and left wheels, respectively.

Using a similar approach to the method in Section 1.4 of [23] for deriving the nonholonomic dynamics of a vertical rolling disk, we eliminate the Lagrange multipliers from these equations to obtain the unconstrained equations of motion for the robot's core. Since $rank(\boldsymbol{A}_c) = 3$, the four constraint equations (37) are linearly dependent, and the number of linearly independent constraints is 3. These three constraints can be calculated from basic row operations on the matrix $\boldsymbol{A}_c$ in Eq. (38). By adding the first and third rows and the second and fourth rows of $\boldsymbol{A}_c$, we obtain the following two equations from Eq. (37):

$$\dot{x} = \frac{r}{2}(\dot{\theta}_R + \dot{\theta}_L)\cos(\theta)\;, \quad \dot{y} = \frac{r}{2}(\dot{\theta}_R + \dot{\theta}_L)\sin(\theta). \quad (40)$$

Subtracting the third row of $\boldsymbol{A}_c$ from the first row (or the fourth row from the second row) yields the third equation:

$$\dot{\theta} = \frac{r}{2b}(\dot{\theta}_R - \dot{\theta}_L). \quad (41)$$

Eq. (40)–Eq. (41) are the three linearly independent constraint equations. Differentiating these equations with respect to time, and substituting the resulting expressions for $\ddot{x}$, $\ddot{y}$, and $\ddot{\theta}$ into the first, second, and third equations in Eq. (39), we obtain:

$$\begin{aligned} &\frac{r}{2}\left(\cos(\theta)(\ddot{\theta}_R + \ddot{\theta}_L) - \dot{\theta}\sin(\theta)(\dot{\theta}_R + \dot{\theta}_L)\right) = \frac{1}{m_c}(\lambda_1 + \lambda_3) \\ &\frac{r}{2}\left(\sin(\theta)(\ddot{\theta}_R + \ddot{\theta}_L) + \dot{\theta}\cos(\theta)(\dot{\theta}_R + \dot{\theta}_L)\right) = \frac{1}{m_c}(\lambda_2 + \lambda_4) \\ &\frac{r}{2b}I_c(\ddot{\theta}_R - \ddot{\theta}_L) = b\cos(\theta)(\lambda_1 - \lambda_3) + b\sin(\theta)(\lambda_2 - \lambda_4). \end{aligned} \quad (42)$$

Adding the fourth and fifth equations in Eq. (39) results in the equation:

$$\begin{aligned} J_w(\ddot{\theta}_R + \ddot{\theta}_L) = \;& (\tau_R + \tau_L) - r\cos(\theta)(\lambda_1 + \lambda_3) \\ & - r\sin(\theta)(\lambda_2 + \lambda_4). \end{aligned} \quad (43)$$

By substituting in the expressions for $\lambda_1 + \lambda_3$ and $\lambda_2 + \lambda_4$ from Eq. (42), we obtain:

$$\left(J_w + \frac{m_c r^2}{2}\right)(\ddot{\theta}_R + \ddot{\theta}_L) = \tau_R + \tau_L. \quad (44)$$

Subtracting the fifth equation from the fourth equation in Eq. (39), we have:

$$\begin{aligned} J_w(\ddot{\theta}_R - \ddot{\theta}_L) = \;& (\tau_R - \tau_L) - r\cos(\theta)(\lambda_1 - \lambda_3) \\ & - r\sin(\theta)(\lambda_2 - \lambda_4). \end{aligned} \quad (45)$$

If we move the term $(\tau_R - \tau_L)$ to the left-hand side of the above equation, then the right-hand side is equal to the right-hand side of the third equation in Eq. (42) multiplied by $-r/b$. Therefore, Eq. (45) can be rewritten as:

$$\left(J_w + \frac{r^2}{2b^2}I_c\right)(\ddot{\theta}_R - \ddot{\theta}_L) = \tau_R - \tau_L. \quad (46)$$

The Lagrange multipliers, *i.e.* the elements of $\boldsymbol{\lambda}$, have been eliminated in Eq. (44) and Eq. (46). Also, since the number of original generalized coordinates is 5 and the number of linearly independent constraints is 3, the robot's core has only 2 degrees of freedom, and the unconstrained dynamics of the core are therefore expressed by two equations. Hence, Eq. (44) and Eq. (46) are the unconstrained equations of motion for the robot's core. Finally, defining

$$H_1 = J_w + \frac{m_c r^2}{2}, \quad H_2 = J_w + \frac{r^2}{2b^2}I_c, \quad (47)$$

we can write Eq. (44) and Eq. (46) in matrix form:

$$\begin{bmatrix} H_1 & H_1 \\ H_2 & -H_2 \end{bmatrix}\begin{bmatrix} \ddot{\theta}_R \\ \ddot{\theta}_L \end{bmatrix} = \begin{bmatrix} 1 & 1 \\ 1 & -1 \end{bmatrix}\begin{bmatrix} \tau_R \\ \tau_L \end{bmatrix}. \quad (48)$$

By pre-multiplying this equation by the inverse of the matrix that multiplies the vector $[\tau_R \;\; \tau_L]^T$, it can be rewritten as

$$\frac{1}{2}\begin{bmatrix} H_1 + H_2 & H_1 - H_2 \\ H_1 - H_2 & H1 + H_2 \end{bmatrix}\begin{bmatrix} \ddot{\theta}_R \\ \ddot{\theta}_L \end{bmatrix} = \begin{bmatrix} \tau_R \\ \tau_L \end{bmatrix}, \quad (49)$$

which is in the standard form of unconstrained dynamics. This formulation shows that $\boldsymbol{q}_c^* = [\theta_R \;\; \theta_L]^T \in \mathbb{R}^2$ is an unconstrained configuration space for the dynamics of a nonholonomic robot.